Comparing symmetry energy predictions and recent constraints from the ASY-EOS experiment at GSI

Francesca Sammarruca

Phys. Rev. C **95**, 044316 — Published 19 April 2017

DOI: 10.1103/PhysRevC.95.044316

Comparing symmetry energy predictions and recent constraints from the ASY-EOS experiment at GSI

Francesca Sammarruca
Physics Department, University of Idaho, Moscow, ID 83844-0903, U.S.A.
(Dated: March 10, 2017)

Predictions for the interaction part of the symmetry energy obtained from microscopic approaches based upon different foundations are reviewed and discussed in the light of recent updated constraints obtained from reaction observables in the ASY-EOS experiment at GSI. The discussion is then extended to the neutron skin thickness in ^{208}Pb and its relation to the density derivatives of the symmetry energy at and below saturation density. With regard to the latter, the main point is to demonstrate the importance of proper consideration of the theoretical uncertainties of microscopic predictions in order to guide phenomenological analyses.

I. INTRODUCTION

The importance of the symmetry energy for the properties of neutron-rich systems cannot be overstated. At the same time, knowledge of this quantity remains limited, particularly its density dependence above saturation. The issue of whether a "soft" or "stiff" density dependence of the symmetry energy is more consistent with available constraints continues to be discussed extensively in the literature, see, for instance, Refs. [1–3] and references therein.

Constraints are typically extracted from heavy ion collision observables, although nuclear data and other types of experiments have been used as well [4]. The neutron-proton elliptic flow ratio and difference are among the observables found to be sensitive to the density dependence of the symmetry energy [5, 6]. Comparison of data from the FOPI-LAND experiment [7, 8] with transport model calculations [9–11] suggested a softer-than-linear to linear term for the potential energy part of the symmetry energy, when the latter is parametrized as a power law.

In a recent paper [12], results from the ASY-EOS experiment at GSI were reported. The measured observables are the directed and elliptic flows of neutrons and light charged particles in the reaction ^{197}Au + ^{197}Au at 400 MeV per nucleon. The findings confirm the moderately soft to linear density dependence from the FOPI-LAND experiment, but in Ref. [12] the authors are also able to extract a more stringent constraint up to twice normal density. Naturally, when new or updated constraints become available, comparison with microscopic calculations is more timely than ever. Within that spirit, modern predictions of the symmetry energy based on chiral effective field theory (EFT) [13, 14] are reviewed and discussed.

It is not among the paper's scopes to give a detailed review of how nuclear forces are derived within chiral EFT. Comprehensive review articles can be consulted for that purpose (see, for instance, Ref. [15] and references therein). Only the main features and strength of chiral EFT will be recalled: it is firmly based on the symmetries of low-energy quantum chromodynamics (QCD), and the predictions can be improved in a systematic way. For these reasons, at this time chiral EFT is the most fundamental and potentially model independent approach to developing nuclear forces.

For comparison, more "traditional" approaches are also included in this study, such as those based on meson-theoretic or phenomenological nucleon-nucleon (NN) potentials and three-nucleon forces (3NF). These approaches, which were particularly popular in the 1990's and are still frequently used today, follow a very different philosophy. Thus, their inclusion in the comparison can be both interesting and insightful.

This paper is organized in the following way: In the next section, some basic phenomenological features of the equation of state (EoS) of isospin-asymmetric matter and the symmetry energy will be reviewed. I will then proceed to describe briefly how the various theoretical EoS used here are generated. In Section III, the density dependence of the potential part of the symmetry energy as predicted by the various approaches under consideration are discussed and compared specifically in the light of the recent constraints. At this point the study is extended to theoretical predictions of the neutron skin thickness in ^{208}Pb in comparison with those extracted using the recent symmetry energy constraints. *The main point of this discussion, as well as of the paper, is to demonstrate the importance of including microscopic predictions when correlating the density dependence of the symmetry energy (namely, its density derivative) to the neutron skin thickness. More precisely, I wish to address the following questions: How consistent with the constraints are the theoretical predictions? How do consistencies or inconsistencies impact the possibility to constrain the density dependence of the symmetry energy at saturation from an accurate knowledge of the neutron skin in ^{208}Pb?*

A brief summary and conclusions are contained in Sect. IV

II. THE EQUATION OF STATE OF ASYMMETRIC NUCLEAR MATTER AND THE SYMMETRY ENERGY.

A. Simple facts and phenomenology

Neglecting powers beyond α^2, where α is the neutron asymmetry parameter defined in terms of the neutron and proton densities, ρ_n and ρ_p, as $(\rho_n - \rho_p)/(\rho_n + \rho_p)$, the EoS of isospin-asymmetric nuclear matter is written as

$$e(\rho, \alpha) = e(\rho, 0) + e_{sym}(\rho)\alpha^2 \ , \tag{1}$$

with $e_{sym}(\rho)$ the symmetry energy. In this approximation, the symmetry energy is then

$$e_{sym}(\rho) = e(\rho, 1) - e(\rho, 0) \ . \tag{2}$$

The well-known expression for the average non-relativistic kinetic energy of nucleons (with mass m) in nuclear matter at some density corresponding to a Fermi momentum k_F is elementary to derive and can be written as

$$T = \frac{3}{10}\frac{k_F^2}{m} \ . \tag{3}$$

Therefore, the kinetic contribution to the symmetry energy is

$$e_{sym}^{kin}(\rho) = e(\rho, 1)^{kin} - e(\rho, 0)^{kin} = \frac{3}{10m}[(k_F^n)^2 - k_F^2] \ , \tag{4}$$

where the neutron Fermi momentum in neutron matter, k_F^n, is related to the Fermi momentum in symmetric nuclear matter at the same density as $k_F^n = 2^{1/3}k_F$. In terms of the Fermi energy, E_F, one can write

$$e_{sym}^{kin}(\rho) = \frac{3}{5}E_F(2^{2/3} - 1) \ . \tag{5}$$

Expressing the Fermi energy in terms of ρ/ρ_0, where ρ_0 is about 0.16 fm^{-3}, one finds

$$e_{sym}^{kin}(\rho) = T_0\Big(\frac{\rho}{\rho_0}\Big)^{2/3} \ , \tag{6}$$

where the value of the coefficient T_0 can be easily verified to have a value around 12-13 MeV. The parametrization used in the analysis of Ref. [12] is

$$e_{sym}(\rho) = 22 \text{ MeV}\Big(\frac{\rho}{\rho_0}\Big)^{\gamma} + 12 \text{ MeV}\Big(\frac{\rho}{\rho_0}\Big)^{2/3} \ , \tag{7}$$

which fixes the symmetry energy at ρ_0 to be 34 MeV. The power law coefficient, γ, is reported as 0.72 ± 0.19. From the FOPI-LAND experiment [7, 8], the same coefficient was found to be 0.9 ± 0.4.

B. Theoretical input

1. *The chiral EoS*

First, I obtain the symmetry energy from the microscopic EoS of symmetric nuclear matter and the one of pure neutron matter based on chiral EFT and calculated as described in Ref. [16]. The predictions at next-to-next-to-next-to-leading order (N^{3}LO) and at next-to-next-to-leading order (N^{2}LO) are based on high-precision chiral nucleon-nucleon (NN) potentials at the respective orders [15, 18] together with the leading 3NF, which is treated as in Ref. [19]. After subtracting the kinetic energy (as given in Eq. (5)) from the symmetry energy, the microscopic values of the potential energy part are fitted with a power law, $V_0(\rho/\rho_0)^{\gamma}$, where, for each of the models being considered, ρ_0 is the actual saturation density for that particular EoS.

One of the important features of chiral EFT is the possibility to estimate the truncation error at each order of the chiral expansion. The truncation error at order n is a measure of what is left out when the chiral expansion terminates at order n. If the prediction for observable X at order $n+1$ is known, the truncation error at order n is

$$\epsilon_n = |X_{n+1} - X_n| \ , \tag{8}$$

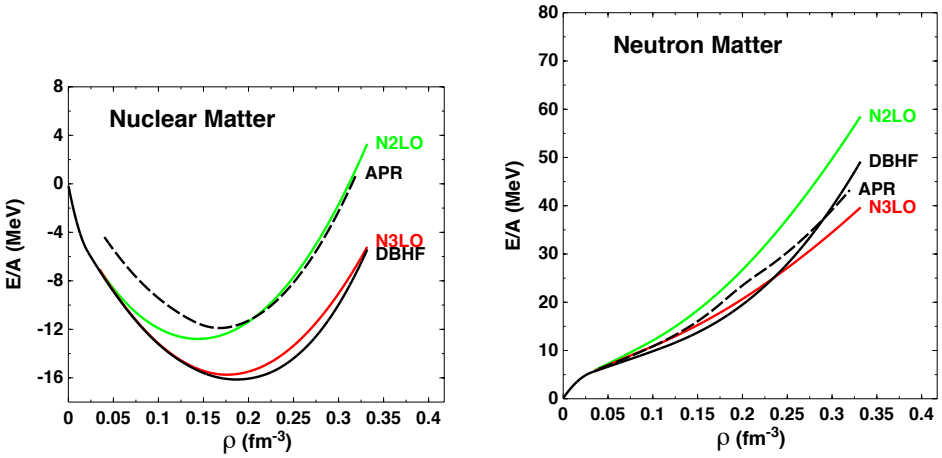

FIG. 1: (Color online) The EoS of symmetric matter (left side) and of neutron matter (right side) for the theories and models considered in this study.

which is the same as the $(n+1)^{th}$ correction. On the other hand, if X_{n+1} is unknown, the truncation error can be estimated to be

$$\epsilon_n = |X_n - X_{n-1}| \frac{Q}{\Lambda} \,, \tag{9}$$

where Q is a momentum typical for the system under consideration (or the pion mass), and Λ is the cutoff parameter of the regulator, which is 450 MeV for the chiral potentials applied in the present work.

In the following, the error is estimated according to Eq. (9), with Q taken to be the Fermi momentum corresponding to the appropriate density of nucleonic matter. A different prescription is proposed in Ref. [17]. Since estimating the truncation error at N^{3}LO requires the predictions at N^{2}LO, those will be shown as well. (N^{4}LO predictions are not yet available.) Note that the N^{2}LO calculation is complete, in the sense that both the two-nucleon force (2NF) and the 3NF are consistently at next-to-next-to-leading order. This is not the case, though, for the N^{3}LO calculation, where the 3NF at N^{2}LO is employed. Efforts are in progress to remove this inconsistency.

2. Relativistic meson-theoretic potentials and the Dirac-Brueckner-Hartree-Fock approach to the equation of state

The relativistic approach to nuclear matter, particularly the Dirac-Brueckner-Hartree-Fock (DBHF) approximation, was developed in the 1980's [20–23]. The starting point was the observation that the DBHF theory, unlike conventional Brueckner theory, had the inherent ability to describe successfully the saturation properties of nuclear matter, that is, saturation energy and density of the EoS. The DBHF method describes the nuclear mean field in terms of strong scalar and vector components that, together, account for the binding of nucleons as well as the large spin-orbit splitting seen in nuclear states. The characteristic feature of the DBHF approach is the fact that important 3NF are effectively taken into account through the density dependence of the nucleon spinors. This effective 3NF, which originates from virtual excitations of nucleon-antinucleon pairs and is, for that reason, known as "Z-diagrams", provides a powerful saturating effect and, thus, an important missing mechanism in conventional Brueckner-Hartree-Fock calculations. For recent reviews, including considerations of isospin asymmetry, see Refs. [24, 25].

3. Variational approaches

Alternatively, the energy per particle in nuclear matter can be obtained combining the 2NF with meson-theoretic or phenomelogical 3NF to generate the additional repulsion essential to improve saturation. Nonrelativistic calculations of symmetric and neutron matter based on variational methods [26] and phenomenological 2NF and 3NF have been used extensively. To also represent this point of view, I will include predictions [27] based on popular phenomenological

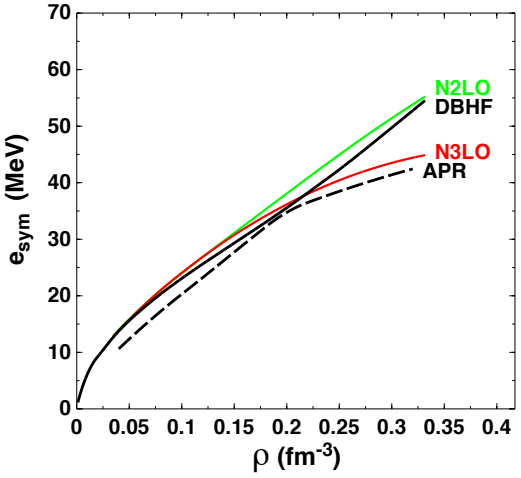

FIG. 2: (Color online) As in Fig. 1, but for the symmetry energy.

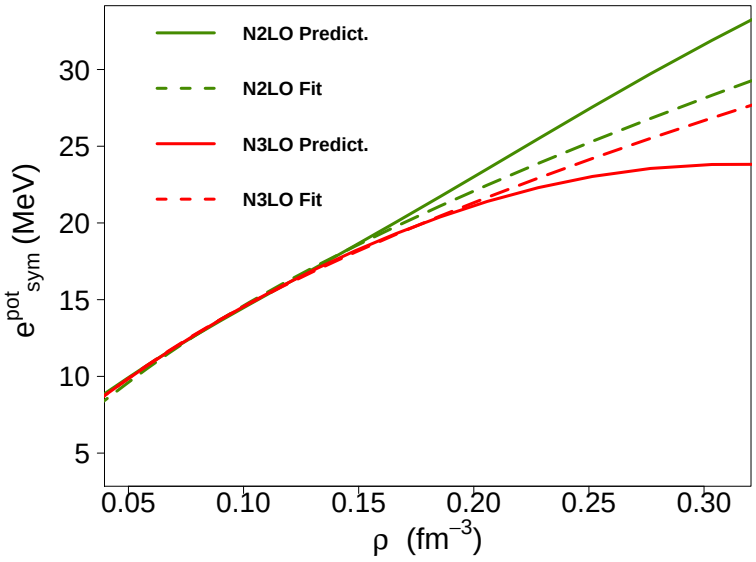

FIG. 3: (Color online) Microscopic predictions of the interaction part of the symmetry energy at N^2LO and N^3LO of chiral perturbation theory, and corresponding power-law fits. See inset for the definition of the various curves.

2NF and 3NF from the 90's, namely the Argonne v_{18} NN potential [28] together with the Urbana model IX [29] 3NF. These will be referred to as the "APR" model.

III. PREDICTIONS AND DISCUSSION

This section opens with an overview of the energy per particle in symmetric nuclear matter (SNM) and pure neutron matter (NM) for the theories and models included in this investigation, see Fig. 1. In Fig. 2, the corresponding values

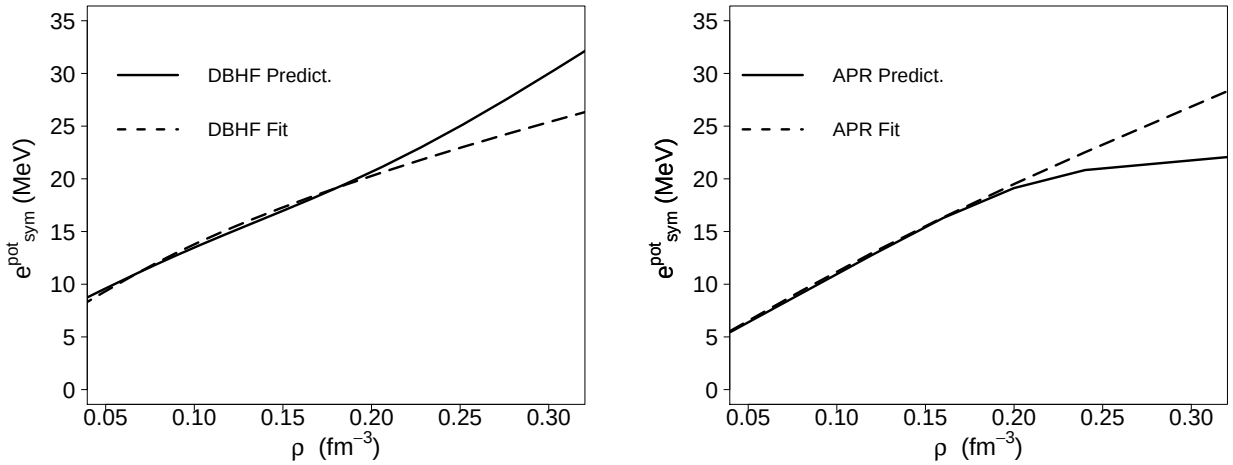

FIG. 4: (Color online) Left: The potential part of the symmetry energy as predicted with the DBHF calculation compared with a power-law fit. Right: The same, but for the APR model [27].

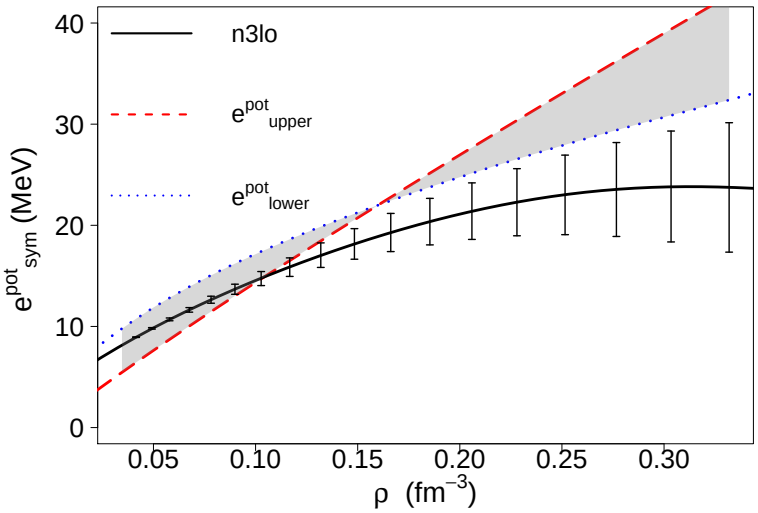

FIG. 5: (Color online) Microscopic predictions of the interaction part of the symmetry energy at N^{3}LO with EFT truncation error. The shaded area shows the empirical constraint from Ref. [12].

for the symmetry energy is displayed, revealing considerable model dependence, especially at and above saturation.

Turning attention to the potential energy part of the symmetry energy, in Fig. 3 I display this quantity as obtained from microscopic calculations at N^{2}LO (solid green line) and at N^{3}LO (solid red line), together with approximations given by functions of the form

$$e_{sym}^{pot} = V_0(\rho/\rho_0)^\gamma \ , \tag{10}$$

dashed green for N^{2}LO and dashed red for N^{3}LO. The fit is done by searching for the single parameter γ, setting V_0 equal to the microscopically predicted value at ρ_0. The density range considered in the fit covers approximately from 0.03 to 0.33 fm^{-3}, with all points carrying the same weight.

Theoretical approach	γ	γ (reduced density range)
N^2LO	0.60 ± 0.05	0.58 ± 0.05
N^3LO	0.55 ± 0.03	0.55 ± 0.03
DBHF	0.55	
APR	0.79	

TABLE I: Exponent of the power law, $V_0\left(\frac{\rho}{\rho_0}\right)^\gamma$, fitted to each of the predicted interaction symmetry energies. Note that the chiral results are reported with their truncation error.

Some additional comments are in place at this point concerning the density range used for the fit. Of course there are limitations to the reliability of chiral predictions. Around $2\rho_0$, the neutron Fermi momentum in neutron matter is about 2.1 fm^{-1} or 420 MeV, close to the cutoff of 450 MeV. However, the Fermi momentum is the highest, and not the average or typical momentum of the system. In fact, the *r.m.s.* relative momentum of two nucleons in nuclear matter can be estimated to be 55% of the Fermi momentum. Therefore, the chiral predictions up to that density should be sound. Nevertheless, it is interesting to check how the best-fit γ is impacted if only densities up to about saturation are retained. I find that the outcome is unchanged (to two significant digits) at N^3LO, and changes by about 3% at N^2LO. This may indicate that the presence of "cutoff artifacts" is less likely at the higher order, although the variation is within chiral uncertainty.

Table I displays the exponent of the power law found in each case, including (for the chiral models) those obtained when only densities up to saturation are retained. The theoretical curves appear reasonably described by the simple *ansatz* up to their respective saturation densities and somewhat above it, whereas the constraint should be applicable up to about $2\rho_0$, which amounts to approximately 0.3 fm^{-3} by the definition of Ref. [12]. Furthermore, an analytical approximation which appears reasonable may be less than satisfactory with respect to derivatives. This point will be addressed again later in the paper.

As in the previous figure, in Fig. 4 one can see to which degree the interaction part of the symmetry energy can be approximated by a single-term power law for the Bonn B meson-exchange potential [31] used in a DBHF calculation (left-hand side), while a similar comparison is shown on the right-hand side of the same figure for the potential symmetry energy obtained from the EoS of Ref. [27]. As it turns out, the power law of the predictions is within the range of the empirical constraint of Ref. [12], $\gamma = 0.72 \pm 0.19$, see Table I.

Although the overall quality of these parametrizations does not suggest that they would be a sound replacement for the actual predictions, a few comments may be insightful. For instance, the smaller size of the exponent in the EoS based on the N^3LO NN potential is an indicator of the softer nature of the chiral interaction at N^3LO. The exponent we find for the DBHF curve has the same value, but note that, in this case, the fitting function underestimates the actual predictions at the higher densities, whereas it overshoots them in the N^3LO case, as the two (exact) curves depart from each other with increasing density.

It is important to note that the N^3LO predictions must be seen in the context of EFT theoretical uncertainties. Therefore, in Fig. 5 the N^3LO predictions are shown with their estimated truncation error calculated as in Eq. (9), with Q the Fermi momentum at each density. At this point, it is also appropriate to recall that there is no well-defined prescription to reliably estimate theoretical errors in cases such as DBHF or APR, or, for that matter, any approach that is not EFT-based. In Fig. 5, the shaded area represents the empirical constraint. The predictions fall within the empirical constraints at subsaturation densities but are otherwise softer.

Obviously, the parametrization given in Eq. 7 was found to be consistent with the reaction observables measured in the GSI experiment. However, here one learns that, although a moderately soft (less than linear) dependence is preferred by microscopic models, Eq. 7 is overall not a satisfactory representation of these theoretical predictions. It would be interesting to move beyond the power-law parametrization when analyzing elliptic-flow ratios. We will come back to this point at the end of this Section, armed with more information.

An "observable" which has been identified as sensitive to the density dependence of the symmetry energy is the neutron skin thickness. Therefore, next we extend the discussion to the neutron skin of ^{208}Pb in relation to density derivatives and pressure. Neutron skins are calculated as described in some recent papers [34, 35], which are based on an earlier work [36]. Namely, the parameters of the proton and neutron distributions, from which the skin is obtained, are extracted by minimizing the energy of a nucleus which is written in terms of a liquid-drop functional. As input to the functional, one needs the EoS of asymmetric matter, Eq. (1), to be constructed in accordance with Eq. (1). First, the EoS will be built using empirical parametrizations taken from Ref. [37] or Ref. [38] for the isospin-symmetric part, whereas the symmetry energy is as in Eq. (7). The saturation density of these phenomenological parametrizations is approximately equal to 0.16 fm^{-3}, consistent with the one used in the ASY-EOS analysis.

γ	S (fm)	$\frac{\partial e_{sym}}{\partial \rho}$ (MeV fm^3)	L (MeV)	P_0 (MeV/fm^3)
0.53	0.14	154	60.1	3.14
0.72	0.18	177	72.6	3.80
0.91	0.21	195	85.2	4.45

TABLE II: Neutron skin (S) of ^{208}Pb with varying power law, γ, in the interaction symmetry energy within the range determined by the ASY-EOS analysis. The third column displays the the slope of the symmetry energy at about 2/3 of saturation density, followed by the L parameter and the symmetry pressure. For further details, see discussion in the text.

I consider three different parametrizations of the symmetric matter EoS: the one from Ref. [37], fitted to K_0=240 MeV, where K_0 is the incompressibility of nuclear matter, and those from Ref. [38], with $K_0 = (240 \pm 20)$ MeV. The values shown here are averages within the range allowed by the uncertainties, which are estimated as in Refs. [34, 35]. For the skin thickness, the compounded error arising from the method I use to compute the skin is about $\pm$ 0.01 fm [35]. For each γ, the density derivatives and pressure also carry uncertainty due to small variations in ρ_0, which impact the kinetic energy coefficient in Eq. (6). Those differences, however, are much smaller than the ones originating from the uncertainty in γ (or, from the choice of the theoretical approach, as will be shown later).

In Table II, for values of γ spanning the uncertainty of the ASY-EOS constraint, I show (second, fourth, and fifth columns, respectively), the skin thickness of ^{208}Pb, the L parameter, defined as

$$L = 3\rho_0 \Big(\frac{\partial e_{sym}}{\partial \rho}\Big)_{\rho_0} \tag{11}$$

through a well-known expansion of the symmetry energy around saturation density, and the symmetry pressure, $P_0 = \rho_0 L/3$. For a family of such simple models, differing only in the density dependence of the potential part of the symmetry energy through the power law, one finds a very strong correlation between the skin and L. This confirms that the skin is sensitive to the pressure in the neutron-rich matter at the core of ^{208}Pb which pushes excess neutrons towards the low-density edges of the nucleus.

On the other hand, the average density in nuclei is less than saturation density and, therefore, typical nuclear observables (such as, for instance, those used to construct phenomenological forces) actually probe lower densities. In this regard, it has been observed [32] that, when values of the neutron skin within a certain range are included as additional constraints in the development of Skyrme forces, the resulting symmetry energies obtained with these adjusted forces are all rather similar around ρ=0.1 fm^{-3} (about 2/3 of normal density and closer to the average density of nuclei), whereas the slopes at the same point differ considerably. This suggests that a very precise value of the skin is necessary to constrain the density slope and thus allow a reliable extrapolation to normal nuclear densities. With these comments in mind, Table II also shows how the slope of the symmetry energy at ρ=0.1 fm^{-3} varies in relation to the neutron skin (third column).

Some of the observations collected above can be summarized as

$$S_{empirical} \approx (0.18^{+0.03}_{-0.04})\ \text{fm}; \quad \Big(\frac{\partial e_{sym}}{\partial \rho}\Big)_{\frac{2}{3}\rho_0} \approx (177^{+18}_{-23})\ \text{MeV fm}^3\ ; \quad L \approx (72.6 \pm 13)\text{MeV}\ . \tag{12}$$

Next, the focus will move on to the four theoretical approaches under the present consideration. At this time, I wish to keep the focus on the impact of the microscopic neutron matter EoS on the neutron skin. Therefore, the EoS of symmetric matter is kept fixed to an empirical one, as used for Table II, whereas the various neutron matter EoS will be the theoretical ones shown on the right-hand side of Fig. 1. Another reason for doing so, besides the just stated fact that I wish to isolate the role of the microscopic NM EoS for the present investigation, is the consideration made in Section II B 1 concerning the missing 3NF in the calculations at N^{3}LO. This contribution has been included in Ref. [33], where it is also confirmed that the impact of the missing 3NF at N^{3}LO in NM is small [33] for the chiral potentials employed here. The same cannot be argued at this time for nuclear matter, and thus the absence of 3NF at N^{3}LO may potentially impact the conclusions of this study, especially when comparing different orders in chiral EFT.

As done above, the uncertainties carried by the energy functional and the choice of the phenomenological EoS of symmetric matter are accounted for. The (averaged) results displayed for the neutron skin carry an approximate uncertainty of 0.01 fm. Those results are found in Table III, along with the predicted values for the same quantities previously reported in Table II.

The spreading of the predictions from the "family" of models in Table III can be summarized as

$$S_{Theories} \approx (0.18 \pm 0.02)\ \text{fm}; \quad \Big(\frac{\partial e_{sym}}{\partial \rho}\Big)_{\frac{2}{3}\rho_0} \approx (154^{+22}_{-19})\ \text{MeV fm}^3\ ; \quad L \approx (58^{+14}_{-11})\text{MeV}\ . \tag{13}$$

Theor. Approach	S (fm)	$\frac{\partial e_{sym}}{\partial \rho}$ (MeV fm^3)	L (MeV)	P_0 (MeV/fm^3)
DBHF	0.16	135	46.8	2.45
N^{3}LO	0.17	148	47.5	2.50
APR	0.18	158	65.0	3.43
N^{2}LO	0.20	176	72.0	3.79

TABLE III: As in Table II, but for each of the theoretical approaches under consideration.

Concentrating on the chiral predictions, the difference between the predictions at N^{2}LO and N^{3}LO is a (pessimistic) estimate of the truncation error at N^{3}LO. As discussed earlier, the truncation error at order n when the prediction at order $n+1$ is unknown is best estimated as in Eq. (9). Taking as Q the Fermi momentum in nucleonic matter corresponding to approximately normal density (or 2/3 of normal density, as appropriate), the chiral predictions at N^{3}LO is estimated to be

$$S_{N3LO} \approx (0.17 \pm 0.02)\ \text{fm}; \quad \Big(\frac{\partial e_{sym}}{\partial \rho}\Big)_{\frac{2}{3}\rho_0} \approx (148 \pm 14)\ \text{MeV fm}^3\ ; \quad L \approx (48 \pm 15)\text{MeV}\ . \tag{14}$$

The additional uncertainty in the skin of about 0.01 fm arising from the theoretical method and mentioned earlier does not increase substantially the compounded uncertainty when added in quadrature to the truncation error. It is noted again that, for non-EFT based predictions (APR and DBHF), a full theoretical uncertainty cannot be reliably estimated.

Earlier I observed, cf. Table II, that very precise measurements of the skin are necessary for a reliable constraint on the density derivative of the symmetry energy. Comparing Table II and Table III, another important point emerges: two values of the skin taken from Table II and Table III, respectively, and being very similar to each other, say within 0.01 fm, correspond to significantly different values of the density derivatives and the L parameter, in particular. In other words, even a very precise measurement of the skin would not be able to contrain the density derivative in a reasonable way when based on simple phenomenological models, such as, for instance, those differing in the exponent of a power law. This point is often overlooked, possibly because analyses of skin *vs.* density-slope are typically conducted within the framework of phenomenology. Furthermore, the result for L at N^{3}LO stated in Eq. (14) is in good agreement with the one reported in Ref. [40], which was also obtained with chiral forces in neutron matter (L = 32.5-57.0 MeV), whereas both are lower than the quoted mean value of 60 MeV typically extracted from reaction data. Based on the evidence shown here, one may conclude that the "discrepancy" resides in the assumed functional form for the interaction symmetry energy, with zero uncertainty near the assumed ρ_0. Such simple form, obviously, cannot capture the details of the density dependence of the theory. It would therefore be better if constraints on the symmetry energy from heavy-ion experiments were expressed as an uncertainty band which allows for diverse functional forms (consistent with theory) and, correspondingly, density derivatives which may cover a broader range than suggested by a power-law assumption.

Additional comments are in place here. In Ref. [12] the authors do mention that the sharp value of $e^{pot}_{sym}(\rho 0)$ is the result of choosing a power law as in Eq. (7) and that using lower values of $e^{pot}_{sym}(\rho 0)$ leads to lower values of L, still within acceptable error margins. However, the results by Brown [32] (which are based on Skyrme phenomenology), are no longer met with the alternative parametrization. The study presented here shows that adhering to Eq. (7) is not recommendable from the theoretical standpoint.

Perhaps the point we set forth to make is more easily captured in a visual way, as presented in Figure 6. The area shaded in blue is obtained from the empirical constraint for L and the corresponding constraint for the neutron skin. Including the predictions from Table III generate the green area. Finally, Eq. (14) produces the pink region. Clearly, the uncertainty in the density derivative is much larger than could be inferred from the blue area.

IV. CONCLUSIONS

The on-going and planned experimental program in nuclear physics is very exciting. Heavy-ion reactions, experiments at radioactive beam facilities, and measurements of the weak charge density in nuclei from the electroweak program at Jefferson laboratory promise to provide, in different ways, new information on neutron-rich systems. In turn, this information will improve current understanding of neutron drip lines, neutron skins, and may potentially reach out to systems of astrophysical relevance, such as neutron stars. Clearly, theoretical calculations are timely and important, in particular from modern *ab initio* predictions

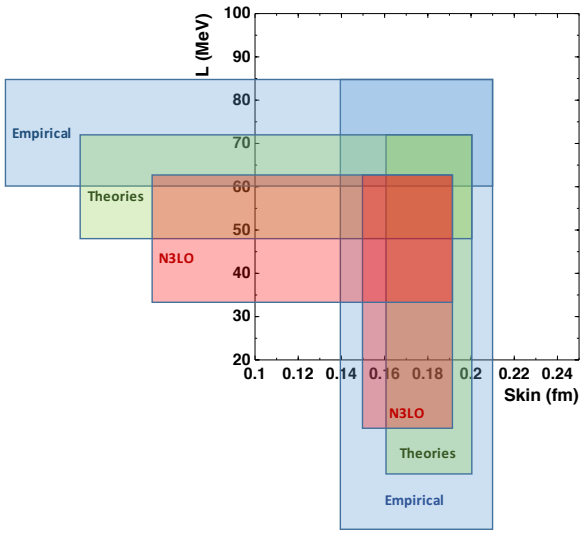

FIG. 6: (Color online) Relation between the L parameter and the neutron skin in ^{208}Pb. Blue shaded area: empirical constraint for L and corresponding constraint for the neutron skin. Green area: Predictions from Table III. Equation (14) produces the pink region.

In this paper, existing predictions for the interaction part of the symmetry energy have been explored in the light of new and more stringent constraints recently obtained for this quantity. I considered a few but fundamentally different approaches to obtain a realistic idea of the spreading in microscopic predictions.

It is important to stress that analyses of reaction observables aimed at extracting constraints on the EoS are not free of assumptions. Within the simplest assumption of a single-term power law, it is found that various predictions based on chiral EFT, relativistic meson-theory, or phenomenological forces and the variational method, can only approximately be described by a power law consistent with the constraint. The latter cannot capture the details of the density dependence of microscopic theories much beyond ρ_0. The N^{3}LO prediction is softer than the constraint at and above saturation density.

The focus then moves to the neutron skin thickness of ^{208}Pb. This is obtained using the symmetry energy constraint supplemented with empirical EoS for symmetric matter and compared with the predictions from the various theoretical approches in the purview of this study. To highlight the impact of the neutron matter EoS and its pressure on the formation of the skin, the latter has been calculated with microscopic predictions of the NM EoS while the EoS for SNM remained fixed by empirical information.

Hopefully, very precise measurements of the skin will be delivered by new PREX experiments which may, in turn, provide reasonable constraints on the density dependence of the NM EOS below and around saturation density. In that regard, this paper aims at demonstrating the importance of experiments keeping in close touch with ab initio predictions. Caution must be excercised with regard to the possibility of constraining the density slope from the knowledge of the skin based only on correlations obtained with families of simple phenomenological interactions. As shown, the latter procedure may underestimate the uncertainties.

Acknowledgments

This work was supported by the U.S. Department of Energy, Office of Science, Office of Basic Energy Sciences, under Award Number DE-FG02-03ER41270. I thank R. Millerson for help with graphics.

---

[1] F. Sammarruca, Symmetry **2014**, 6(4), 851.
[2] J.M. Lattimer and Y. Lim, Astrophys. J. **771**, 51 (2013).
[3] M. Baldo and G.F. Burgio, arXiv:1606.08838.
[4] M.B. Tsang *et al.*, Phys. Rev. C **86**, 015803 (2012); and references therein.
[5] P. Russotto *et al.*, Phys. Lett. **B 697**, 471 (2011).
[6] M.D. Cozma, Phys. Lett. **B 700**, 139 (2011).
[7] Y. Leifels *et al.* Phys. Rev. Lett. **71**, 963 (1993).
[8] D. Lambrecht *et al.*, Z. Phys. **A 350**, 115 (1994).
[9] Qingfeng Li, Zhuxia Li, S. Soff, R.K. Gupta, M. Bleicher, and H. Stöcker, J. Phys. G **31**, 1359 (2005).
[10] Q. Li, Z. Li, S. Soff, M. Bleicher, and H. Stöcker, J. Phys. G **32**, 151 (2006).
[11] Q. Li, Z. Li, S. Soff, M. Bleicher, and H. Stöcker, J. Phys. G **32**, 407 (2006).
[12] P. Russotto *et al.*, Phys. Rev. C **94**, 034608 (2016).
[13] S. Weinberg, Physica **96A**, 327 (1979).
[14] S. Weinberg, Phys. Lett. B **251**, 288 (1990).
[15] R. Machleidt and D.R. Entem, Phys. Rep. **503**, 1 (2011).
[16] F. Sammarruca, L. Coraggio, J. Holt, N. Itaco, R. Machleidt, and L.E. Marcucci, Phys. Rev. C **91**, 054311 (2015).
[17] E. Epelbaum, H. Krebs, and U.-G. Meissner, Eur. Phys. J. A **51**, 53 (2015).
[18] D.R. Entem and R. Machleidt, Phys. Rev. C **68**, 041001 (2003).
[19] J.W. Holt, N. Kaiser, and W. Weise, Phys. Rev. C **79**, 054331 (2009); Phys. Rev. C **81**, 024002 (2010).
[20] M.R. Anastasio, L.S. Celenza, W.S. Pong, and C.M. Shakin, Phys. Rep. **100** (1983) 327.
[21] C.J. Horowitz and B.D. Serot, Phys. Lett. **137B** (1984) 287; Nucl. Phys. **A464** (1987) 613.
[22] R. Brockmann and R. Machleidt, Phys. Lett. **149B** (1984) 283; Phys. Rev. C **42** (1990) 1965.
[23] B. ter Haar and R. Malfliet, Phys. Rep. **149** (1987) 207.
[24] F. Sammarruca, Int. J. Mod. Phys. E **19** (2010) 1259.
[25] H. Müther, F. Sammarruca, and Z. Ma, arXiv: 1611.05621 [nucl-th]; Int. J. Mod. Phys., in press.
[26] A. Akmal and V.R. Pandharipande, Phys. Rev. C **56**, 2261 (1997).
[27] A. Akmal, V.R. Pandharipande, and D.G. Ravenhall, Phys. Rev. C **58**, 1804 (1998).
[28] R.B. Wiringa, V.G.J. Stoks, and R. Schiavilla, Phys. Rev. C **51**, 38 (1995).
[29] B.S. Pudliner, V.R. Pandharipande, J. Carlson, and R.B. Wiringa, Phys. Rev. Lett. **74**, 4396 (1995).
[30] C. Fuchs and H.H. Wolter, Eur. Phys. J. A **30**, 5 (2006).
[31] R. Machleidt, Adv. Nucl. Phys. **19**, 189 (1989).
[32] B.A. Brown, Phys. Rev. Lett. **111**, 232502 (2013).
[33] C. Drischler, A. Carbone, K. Hebeler, and A. Schwenk, arXiv: 1608.05615 [nucl-th].
[34] F. Sammarruca and Y. Nosyk, Phys. Rev. C **94**, 044311 (2016).
[35] F. Sammarruca, Phys. Rev. C **94**, 054317 (2016).
[36] D. Alonso and F. Sammarruca, Phys. Rev. C **68**, 054305 (2003).
[37] N. Alam, B.K. Agrawal, J.N. De, S.K. Samaddar, G. Coló, Phys. Rev. C **90**, 054317 (2014).
[38] LieWen Chen, arXiv:0910.0086 [nucl-th]; Sci. China **G52**, 1494 (2009).
[39] K. Oyamatsu, Kei Iida, and Hiroyuki Koura, Phys. Rev. C **82**, 027301 (2010).
[40] K. Hebeler and A. Schwenk, Eur. Phys. J. A **50**, 11 (2014).